arXiv:1612.00468v3 [astro-ph.HE] 24 Jan 2017

Energetics and Birth Rates of Supernova Remnants in the Large Magellanic Cloud

D.A. Leahy
Department of Physics & Astronomy, University of Calgary, Calgary, Alberta T2N 1N4, Canada

ABSTRACT

Published X-ray emission properties for a sample of 50 supernova remnants (SNRs) in the LMC are used as input for SNR evolution modelling calculations. The forward shock emission is modelled to obtain the initial explosion energy, age, and circumstellar medium density for each SNR in the sample. The resulting age distribution yields a SNR birthrate of 1/(500 yr) for the LMC. The explosion energy distribution is well fit by a log-normal distribution, with most-probable explosion energy of 0.5×10^{51}erg, with a 1-σ dispersion by factor 3 in energy. The circumstellar medium density distribution is broader than the explosion energy distribution, with most-probable density of $\sim$0.1 cm^{-3}. The shape of the density distribution can be fit with a log-normal distribution, with incompleteness at high density caused by shorter evolution times of SNRs.

Subject headings: supernova remnants: general

1. Introduction

The study of supernova remnants (SNRs) is of great interest in astrophysics. SNRs can provide valuable information relevant to their stellar progenitors and the associated explosion events that end their stellar lives. The hot shocked gas in the interior of a SNR is observed in X-rays, with a temperature $\sim$1 keV. This temperature is determined by the physics of shocks and the evolutionary history of the interior of the supernova remnant. Models, based on hydrodynamic simulations, can be constructed which represent a reasonable approximation of the evolution of a supernova remnant (e.g. Truelove & McKee (1999), Cioffi et al. (1988)). Such models, together with the observed X-ray emission, can be used to deduce the explosion energy and the age of the SNR and the density of its surroundings. A study of a large number of SNRs can yield insights about the physical processes related to SNR, such as SNR evolution, SN explosion energies and properties of the environment in which SN explode.

Studies of populations of SNRs have previously been carried out. Here a few recent studies are pointed out. The sizes of SNRs in the LMC and SMC is known to follow a linear cumulative distribution (Bandiera & Petruk (2010) and references therein). Badenes et al. (2010) showed this to be most likely caused by SNRs exploding in an ISM which has a broad density distribution. A separate study by Bandiera & Petruk (2010) had a similar conclusion. Bandiera & Petruk (2010) analysed the radio surface brightness of SNRs in relation to both SNR diameter and local ISM density. They assumed power-law dependencies of the various quantities, including shock radius vs. time, radio surface brightness and probability distribution of densities. By fitting the power-law models to the observed properties of 8 Galactic SNRs, 24 LMC SNRs and 3 SMC SNRs, they were able to put constraints on the radio emission process and show that the "constant-efficiencies" model for radio emission did not fit the data. Asvarov (2014) studied the size distribution of SNRs in M33. SNRs were chosen based on their X-ray hardness ratio to get a sample as free as possible from selection effects. Monte Carlo methods were used to generate model sets of size distributions to compare to the observed distribution. The main

conclusions were that the warm ISM (with density in the range $0.1 - 1$ cm^{-3} has a filling factor of $\sim 90\%$, and the birthrate of SNRs in M33 is $\simeq$7 per 1000 yr.

An important in input required to carry out SNR modelling is the shock radius. This, in turn, requires knowledge of the SNR's distance. For this reason, this work considers SNRs located in the Large Magellanic Cloud (LMC). The distance to the LMC is well determined at 49.97 ± 0.19(statistical) $\pm$ 1.11 (systematic) kpc (Pietrzyński et al. 2013). LMC SNRs also have been observed extensively in X-rays by XMM-Newton (Maggi et al. 2016). Among their important results were: identification of SN type (core collapse or type Ia) for number of SNRs; and measurement of LMC element abundances from SNRs dominated by emission from shocked interstellar medium.

The current paper further analyses the sample of LMC SNRs from Maggi et al. (2016) by applying the models from Truelove & McKee (1999) with some additional extensions and calculations. Section 2 describes the data and the models that are used. Section 3 gives the results for the derived explosion energies, ages and circumstellar medium densities. Section 4 summarizes the results.

2. LMC SNR Data and SNR Evolution Models

Maggi et al. (2016) present the results of extensive XMM-Newton observations of LMC SNRs. They present X-ray images and spectral analysis results for 51 SNRs. From this list we analyse all but SN1987A, for which our models do not apply, leaving a sample of 50 SNRs. The primary data inputs for our analysis come from their Tables C1, E1 and E2. In particular, the quantities of interest here are the outer shock radius, the temperature and the emission measure. The XMM-Newton temperatures and emission measures are generally the best available values for these LMC SNRs. In several cases Chandra images are available with higher spatial resolution. For those cases we use the shock radius from the Chandra images.

For modelling this sample, some simplifying assumptions are made. Spherically symmetric SNR evolution is assumed, which allows use of analytic approximations to SNR evolution models. This assumption could be relaxed if carrying out multi-dimensional hydrodynamic models, but that is beyond the scope of the current work. As discussed in Truelove & McKee (1999), prior to the onset of radiative cooling, spherically symmetric supernova remnant evolution can be described by unified solutions. These are more complex than self-similar solutions, but are analytic in nature. They describe the SNR evolution (forward and reverse shock evolution) throughout the ejecta-dominated and Sedov-Taylor phases as well as the transition between the two phases. For the transition from Sedov-Taylor phase to the radiative phase the models of Cioffi et al. (1988) are used. For the circumstellar medium, a uniform density is assumed. The ejecta density profiles are taken as power-law in radius with index n Truelove and McKee (1999) present models for n=0 up to n=14 ($n \neq 5$). $n = 7$ is expected for a Type Ia explosion (Colgate & McKee 1969) and $n > 5$ for core collapse supernovae (Chevalier & Fransson 1994).

The model emission measures for material heated by the forward shock, EM, are calculated using the interior SNR structure (density, temperature and pressure profiles): $EM = \int n_e n_H dV$. Dimensionless EM is defined by $dEM = EM/(R_s^3 n_{e,sh} n_{H,sh})$ with post-shock electron density $n_{e,sh} = 4n_e$ and post-shock H density $n_{H,sh} = 4n_H$. n_H and n_e are the preshock (ISM) values, with n_e calculated as if the gas were ionized to the same state as the postshock gas. μ_H and μ_e are the mean molecular weights (or mean masses) per H atom and per electron of the postshock gas. From the definition of mean molecular weights in terms of mass density ρ, $\rho = \mu_H m_H n_H = \mu_e m_H n_e$ one obtains $n_e = \frac{\mu_H}{\mu_e} n_H$. With this definition, dEM is independent of R_s and n_H, and depends only on the shape of the interior density distribution. dEM is a constant for the self-similar phases of the evolution during which the shape of the density does not change. For the Sedov-Taylor phase, the interior structure and dEM for the self-similar solution is calculated using the equations given in White & Long (1991) with the cloud evaporation source term set to zero. For the ejecta dominated phase, dEM is calculated using the self-similar interior solutions given in Chevalier (1982) for n=7 and n=12 cases. Only the part of the self-similar solution exterior to the contact discontinuity is used to

obtain dEM of the forward-shocked material. For the transition phase from ejecta self-similar phase to the Sedov-Taylor self-similar phase, dEM is calculated for n=7 and 12 cases as follows. The ejecta self-similar phase ends at time t_{core} and the Sedov-Taylor self-similar phase starts at time t_{ST}. t_{core} and t_{ST} are defined and values for different n are given in Truelove & McKee (1999). Between t_{core} and t_{ST}, dEM is interpolated between the ejecta phase value for n=7 or n=12 and the Sedov-Taylor value. Models have been tested for different n on a few SNRs in our sample and it was found that results differ by much less (typically less than a few parts in 1000) than the differences caused by the uncertainties in the input parameters. Thus the presented models are given for the n=7 case. Tests were made using models with different values of ejected mass between 0.5 and 10 $M_{\odot}$. Again, the results differed by much less than differences caused by the uncertainties in the input parameters. Thus the presented models are given for ejected mass of $1.4M_{\odot}$.

The temperature of the X-ray spectrum of the outer shock component of a SNR is the emission-weighted temperature. In the models considered, the temperature increases as radius decreases inside the shock front. Thus the emission-weighted temperature is higher than the temperature at the shock front. At the shock, electrons and ions are heated to different temperatures. The initial heating per particle for a strong shock, with adiabatic index $\gamma = 5/3$ is $\frac{3}{16}\mu m_H V_s^2$. Here μ is the mean molecular weight for the plasma $1/\mu = 1/\mu_{ion} + 1/\mu e$, with μ_{ion} and μ_e, the mean molecular weights for the ions and for the electrons. Mean molecular weights corresponding to LMC abundances are used. These affect the relation between the mass density, number density, pressure and temperature. Thus abundances affect the shock jump conditions, SNR evolution, and emission measures. Details on the SNR models, including effects of abundances, are given in Leahy & Williams (2017).

As the plasma ages the electrons and ions slowly equilibrate in temperature. Ghavamian et al. (2013) gives a detailed discussion of electron ion equilibration. Collisionless shocks are complex, governed by interactions in the plasma which depend on collective processes, and electron heating is not yet well understood. For our main calculations, the calculation of electron heating given in Cox & Anderson (1982) (hereafter CA82) is followed, which uses the results of Itoh (1978). For simplicity, the standard composition $n_{He} = 0.1n_H$ used in CA82, is for the calculation of electron-ion equilibration. Observations of electron to proton temperature ratios in SNRs are relatively recent. Thus an alternate calculation of electron heating is done here using the phenomenological $1/V_s^2$ model (equation 5 in Ghavamian et al. (2013)). The minimum T_e/T_{ion} is set to 0.1 to agree with the observations, which typically have large (factor of 2-5) errors (Fig. 2 in Ghavamian et al. (2013)). The results from the two methods (CA82 and $1/V_s^2$ models) are compared.

For the CA82 calculation, electron-ion temperature equilibration is due to Coulomb collisions. The equilibration timescale is: $t_{eq} = 5000E_{51}^{3/14}n_0^{-4/7}$yr, with E_{51} the explosion energy in units of 10^{51}erg and n_0 the density in cm^{-3}. The electron to ion temperature ratio $\alpha = T_e/T_{ion}$ is given to a good approximation by $\alpha = 1-0.97exp[-(5f/3)^{0.4}(1+0.3(5f/3)^{0.6}]$. Here $f = \frac{ln(\Lambda)}{81}\frac{4n_0}{T_s^{3/2}}(t-t_0)$ with the Coulomb logarithm given by $ln(\Lambda) = ln(1.2\times10^5 T_s^{1/2}T_e(4n_0)^{-1/2})$. t_0 is the time a parcel of gas was shocked and the post-shock density is $4n_0$. The factor of 0.97 in the expression for α has been included to give reasonable agreement with the measured electron to proton temperature ratios for young SNRs (Fig.2 in Ghavamian et al. (2013)). For typical SNR parameters (explosion energy 10^{51} erg, ejected mass of $1.4M_{\odot}$, density of 1 cm^{-3}) our calculations gives $\alpha \simeq 0.055$ for age of 100 yr, increasing rapidly to 0.31 at age of 1000 yr, then more slowly, reaching 0.97 at 5000 yr. To get realistic X-ray (i.e. electron) temperatures from the models, the inclusion of progressive equilibration of electron and ion temperatures is essential.

The ionization states of the ions are generally out of equilibrium with the electron temperature for many SNRs. However, this is already taken into account in modelling the X-ray spectra, so that the electron temperatures derived from the X-ray spectrum are corrected for this effect.

3. Results and Discussion

For each SNR in the LMC with observed radius, R, emission measure, EM, and X-ray temperature, kT, an initial explosion energy, E_0, age, and circumstellar medium density, n_0, were used to calculate a model. The process was iterated until convergence of the output R, EM and kT to the observed values. The procedure is similar to that described in Leahy & Ranasinghe (2016). The resulting E_0, age and n_0 for each of the 50 SNRs is listed in Table 1. The input R is also given. The input EM and kT and their uncertainties are identical to those listed in (Maggi et al. 2016) so are not repeated here. The results from model fitting using the alternate prescription for electron heating show the following differences. Derived density, n_0, is identical. Age on average was smaller by a factor of 0.88 (standard deviation 0.19) and energy larger by a factor of 1.22 (standard deviation 0.52). For SNRs with X-ray temperature < 0.27keV (13 SNRs) there is no significant difference ($< 1\%$ and typically $< 0.1\%$) in age or explosion energy. For X-ray temperature > 0.27keV (37 SNRs), the age is usually smaller, and explosion energy is usually larger. The mean log(age) is 4.12 (1.3×10^4yr) for the CA82 T_e/T_{ion} method and 4.05 (1.1×10^4yr) for the $1/V_s^2$ T_e/T_{ion} method. The mean log($E51$) is -0.293 (5.1×10^{50}erg) for the CA82 T_e/T_{ion} method and -0.144 (7.2×10^{50}erg) for the $1/V_s^2$ T_e/T_{ion} method.

To obtain uncertainties in E_0, n_0, and age, the models were rerun with EM and kT set to the 4 different combinations of upper and lower limits. Then the extreme values of E_0, age and n_0 from this set of fits were used as the upper and lower limits. Generally asymmetric errors on the parameters were obtained, as shown in Table 1 here. The errors in Table one are derived from the errors of the input parameters. An additional systematic error for E_0 and age exists because of the uncertainty in T_e/T_{ion} calculation. A measure of that uncertainty is the standard deviation of difference in results from the two T_e/T_{ion} calculation methods, which is 19% for age and 52% for E_0.

There are wide ranges for the deduced values of E_0, age and n_0. The supernova (SN) explosion energies range from 0.037×10^{51} erg (J0453-6829) to 11×10^{51} erg (J0449-6920), i.e by a factor of 300. Such a wide range should not be surprising: the range in observed SN energies is similarly wide (for Type II SN energies see Rubin et al. (2016)). The deduced ages range from 1300 yr (J0537-6910) to 60,000 yr (J0517-6759). This is in rough agreement with what is expected because SNRs are expected to become too faint to observe after several 10^4 yr. The deduced circumstellar densities range from 0.0007 cm^{-3} (J0505-6753) to 5.5 cm^{-3} (J0453-6655). This spans 4 orders of magnitude and is similar to what is expected for Milky Way SNRs exploding in different environments, ranging from the hot ionized medium, with density $\simeq 0.001 cm^{-3}$, to the diffuse warm and cool HI, with density $\simeq 0.1 - 1 cm^{-3}$, to the molecular medium with density $\geq 1 cm^{-3}$ (Cox 2005).

Plots of the various SNR parameters were made to check that the models gave reasonable results. Fig. 1 shows n_0 vs. age. The SNRs are scattered across the plot except for a clear deficit in the upper-right corner (high density and high age). This absence is expected because the onset of radiative losses occurs earlier for SNR in higher density ISM. The expected transition time to the PDS phase is $t_{PDS} = 13300 (E51)^{3/14} n_0^{-4/7} \zeta_m^{-5/14}$ (CMB88), with ζ_m the metallicity correction to the cooling function. This is plotted in Fig. 1 as the dashed and dotted lines for explosion energies of 10^{50} and 10^{51} erg. SNRs become much fainter as they approach the PDS phase, so the upper limits on the derived ages are consistent with expectations. A plot of explosion energy vs. age shows no correlation. However there is an empty region in the plot at large age and low explosion energy, which is likely because old SNRs with low explosion energy are too faint to be in the sample. The plot of radius vs. age is similar to the plot of radius vs. number because the birthrate of SNRs in the LMC is consistent with a constant value (see below). The reason for the nearly linear trend was discussed in detail by Badenes et al. (2010): it can be well explained by the spread of ISM densities in which SNR explode.

Fig. 2 shows the distribution of SN explosion energies, E_0, derived here for the LMC SNRs. E_0 for each SNR is plotted as a function of cumulative number of SNRs with energy less than or equal to E_0, which is equal to the rank number by energy. The energies are clearly not uniformly distributed, otherwise the slope would be a straight line. Other simple distribution functions, such as

Gaussian in energy, were tested and clearly do not fit the LMC sample values of E_0. Instead the distribution is reminiscent of a log-normal probability distribution:

$$\frac{dN}{dE} = \frac{N_T}{\sqrt{2\pi\sigma^2_{logE}}} e^{-\frac{[log(E)-log(E_{av})]^2}{2\sigma^2_{logE}}} \quad (1)$$

where N_T is the total number in the sample, E_{av} is peak in number vs. energy and σ_{logE} the dispersion in log(E). The solid line in Fig. 1 is the best fit cumulative distribution, with parameters $E_{av} = 0.48 \times 10^{51}$erg and σ_{logE}=0.47. The latter corresponds to a 1-σ dispersion of a factor 2.94 in energy. The process was repeated for the explosion energies derived using the the $1/V_s^2\ T_e/T_{ion}$ method. The plot looks nearly the same as the one in Fig.2. Those energies are also well-fit by a log-normal distribution, but with parameters $E_{av} = 0.54 \times 10^{51}$erg and σ_{logE}=0.50. The latter corresponds to a 1-σ dispersion of a factor 3.16 in energy.

The distribution of SN ages for the LMC SNRs is shown in Fig. 3. Age is plotted for each SNR vs. cumulative number of SNRs with age less than or equal to that of the given SNR. In this case, for ages $\leq$20,000 yr, the distribution is uniformly distributed in age, and is well fit by a straight line. The slope of the line is the birthrate of SNRs in our sample, which corresponds to observable X-ray SNRs in the LMC. The derived birthrate is 1/(503yr), where the fit is done only for SNRs with age $\leq$20,000 yr. The fits were repeated for the ages derived using the the $1/V_s^2\ T_e/T_{ion}$ method. The plot looks nearly the same as the one in Fig.3. The derived birthrate is 1/(507yr), where again the fit is done only for SNRs with age $\leq$20,000 yr.

The excess of ages for rank >40 can be attributed to incompleteness. I.e., because the SNRs with age>20,000 yr are becoming faint, the X-ray surveys are seeing only a fraction of the population. If all of the age>20,000 yr SNRs (say up to 6×10^4yr) were observed, then the rank numbers would be larger, flattening the slope. The incompleteness is estimated by fitting a slope to the set with age rank between 40 and 50. This gives a birthrate of 1/(4200yr), suggesting an incompleteness of a factor of $\simeq$8 for SNRs with age between 20,000 and 60,000 yr compared to those with age $\leq$20,000 yr. Including SN1987A in the sample has the following effect: the birthrate remains at 1/(503 yr) but y-intercept of the line becomes 1060 yr instead of 1560 yr. This suggests that $\sim$2 other young SNRs are missing in the sample, possibly because confusion because of their small size. If the assumption is made that every observable SN produces an observable SNR (for age $\leq$20,000 yr), then the SN rate for the LMC is 1/(500 yr), which is about 1/10 that of the SN rate for the Milky Way. This is roughly consistent with the stellar luminosity of the LMC which is about 1/10 that of the Milky Way. The uncertainties in the SN rate of the Milky Way and the stellar luminosities of the LMC and Milky Way are large enough that a more detailed comparison is not possible.

As a separate test of the derived birthrate, the derived ages were replaced with available estimates from the literature, as summarized in Maggi et al. (2016). Previous estimates were available for 25 LMC SNRs. It was not assessed for each case whether the previous age estimates are more reliable or less reliable than the currently derived ages, in fact many of them are consistent with the same value. A detailed comparison for individual SNRs will be done in future work. The resulting cumulative age distribution looks much the same as that shown in Fig. 2, but the fitted slope is lower, corresponding to a birth-rate of 1/(607 yr). The difference is taken as a measure of the uncertainty in the LMC SNR birthrate, i.e. $\sim$1/(500 yr) to $\sim$1/(600 yr). Future assessment of the methods of obtaining ages should reduce this uncertainty.

Fig. 4 shows the distribution of SNR circumstellar densities, n_0. The densities are clearly not uniformly distributed. Here the n_0 distribution is fit with a log-normal probability function:

$$\frac{dN}{dn_0} = \frac{N_T}{\sqrt{2\pi\sigma^2_{log(n_0)}}} e^{-\frac{[log(n_0)-log(n_{0,av})]^2}{2\sigma^2_{log(n_0)}}} \quad (2)$$

where $n_{0,av}$ is peak in number vs. density and $\sigma_{log(n_0)}$ the dispersion in log(n_0). The fit with a single log-normal distribution is poor but separate fits to the lower and upper sets of densities is good. The solid blue line is the best fit to the 30 lowest densities, with parameters $n_{0,av} = 0.079cm^{-3}$ and $\sigma_{log(n_0}$=0.51. The dashed red line is the best fit to the 30 highest densities, with parameters $n_{0,av} = 0.091cm^{-3}$ and $\sigma_{log(n_0)}$=0.91. The σ's

correspond to 1-σ dispersions of by factors of 3.2 and 8.2 in density. Because the peak densities for both fits are so close to the same value, this suggests that there are not 2 physically distinct distributions of density. One possibility density distribution is not well-described by a log-normal distribution. This may not be surprising considering the complexity of processes that govern the densities in the ISM (e.g. see Cox (2005)). Another possibility is that the high density end of the distribution is under-sampled. SNRs occurring in a high density medium evolve faster and become radiative at earlier times. Thus they would be under-represented in the sample compared to longer-lived SNRs occurring in lower density environments. In this case, the poor fit above density of $\sim 0.2\ cm^{-3}$ would be explained by incompleteness. The mean age for the 30 SNRs with lowest density is 21,000 yr, whereas the mean age of the 20 SNRs with highest density is 12,000 yr. This supports the suggestion that the high density end of the sample is affected by incompleteness.

The density distribution at the sites of SNRs in the LMC has been discussed previously. Badenes et al. (2010) and Bandiera & Petruk (2010) study the size distributions of SNRs in the LMC, SMC and M33. There is a nearly linear size distribution over a fairly wide range in radius (up to 60 pc). Both studies consider SNRs which evolve in a distribution of densities and use this to explain the linear size distribution. The upper cutoff in the size distribution is explained by a minimum in the density distribution (Badenes et al. (2010)) Our result of an approximately log-normal distribution for density is consistent with the linear size distribution of LMC SNRs, because it was derived from nearly the same sample of LMC SNRS as used by Badenes et al. (2010). The density distribution derived here (Fig.3) has been fitted by a n_0^{-1} distribution (the green line in Fig.3), however the log-normal distribution gives a significantly better fit. The reasons that the density distribution here is different the one in Badenes et al. (2010) are: they assumed a power-law density distribution; individual SNRs were modelled here with explosion energy, age and density as parameters for each SNR.

For the current work, the X-ray emission of the forward shock was analysed. It was noted that the results are very insensitive to the amount of ejected mass, M_{ej}, and to the index n for the power-law density distribution of the ejecta. However, the behaviour of the reverse shock is sensitive to both parameters. The SNR evolution model is currently being improved to be able to model the reverse shocked ejecta for values of n between 0 and 14. When the reverse shock model is completed, the X-ray emission from the reverse shock, which is seen in a number of the LMC SNRs, can be modelled. That modelling can yield M_{ej} and n values for a sample of SNRs and will enable us to learn about the properties of the SN progenitors.

4. Summary

X-ray emission properties from the forward shock for a set of 50 SNRs in the LMC has been determined recently by Maggi et al. (2016). Here, SNR evolution and interior structure calculations have been carried out in order to match the observed radius, emission measure and electron temperature for each of the 50 SNRs. The results for explosion energy, age and circumstellar medium density, and their uncertainties, are given in Table 1. T_e/T_{ion} was calculated using the Cox & Anderson (1982) prescription and an additional set of models was calculated using the $1/V_s^2$ prescription (Ghavamian et al. (2013)). The latter gave identical densities, and different ages and explosion energies. However, the analysis of the distributions of ages and explosion energies gave the same results using both methods.

This is the first time that the energy distribution of SNRs, the birthrate of SNRs and the density distribution for SNRs have been measured for any large sample. The distribution of parameters is summarized in Figs. 2, 3 and 4. For explosion energy and density, the distributions were fit by log-normal distributions. A most-probable explosion energy of 0.5×10^{51}erg is found, with a 1-σ dispersion by factor 3 in energy. For density, two log-normal fits are better than one, which may be caused by complexity in the distribution of interstellar medium in the LMC or by incompleteness in the sample. In either case, the mean density is $\sim 0.1 cm^{-3}$ with a 1-σ dispersion by factor $\sim$3-8 in density. For age, incompleteness is clearly a factor for the older part of the sample (age >20,000 yr). For age $\leq$20,000 yr, the ages are well fit by a constant birthrate of 1/(500 yr).

It would be highly desirable to carry out a similar study for Galactic SNRs. One of the main factors limiting such a study is lack of reliable distances to SNRs in the Galaxy. However, once a sample of Galactic SNRs with distances and X-ray observations is obtained, similar modelling can be carried out. Then the properties of Galactic and LMC SNRs can be compared.

D.L. acknowledges the assistance of undergraduate student J.E. Williams, who compiled the LMC data used as input for this study, and also verified some of the model calculations. This work was supported by a grant from the Natural Sciences and Engineering Research Council of Canada.

REFERENCES

Asvarov, A. I. 2014, A&A, 561, A70

Badenes, C., Maoz, D., & Draine, B. T. 2010, MNRAS, 407, 1301

Bandiera, R., & Petruk, O. 2010, A&A, 509, A34

Chevalier, R. A. 1982, ApJ, 258, 790

Chevalier, R. A., & Fransson, C. 1994, ApJ, 420, 268

Cioffi, D. F., McKee, C. F., & Bertschinger, E. 1988, ApJ, 334, 252

Colgate, S. A., & McKee, C. 1969, ApJ, 157, 623

Cox, D. P., & Anderson, P. R. 1982, ApJ, 253, 268

Cox, D. P. 2005, ARA&A, 43, 337

Ghavamian, P., Schwartz, S. J., Mitchell, J., Masters, A., & Laming, J. M. 2013, Space Sci. Rev., 178, 633

Itoh, H. 1978, PASJ, 30, 489

Leahy, D. A., & Ranasinghe, S. 2016, ApJ, 817, 74

Leahy, D. A., & Williams, J. E. 2017, arXiv:1701.05942

Maggi, P., Haberl, F., Kavanagh, P. J., et al. 2016, A&A, 585, A162

Pietrzyński, G., Graczyk, D., Gieren, W., et al. 2013, Nature, 495, 76

Rubin, A., Gal-Yam, A., De Cia, A., et al. 2016, ApJ, 820, 33

Truelove, J. K., & McKee, C. F. 1999, ApJS, 120, 299

White, R. L., & Long, K. S. 1991, ApJ, 373, 543

This 2-column preprint was prepared with the AAS LaTeX macros v5.2.

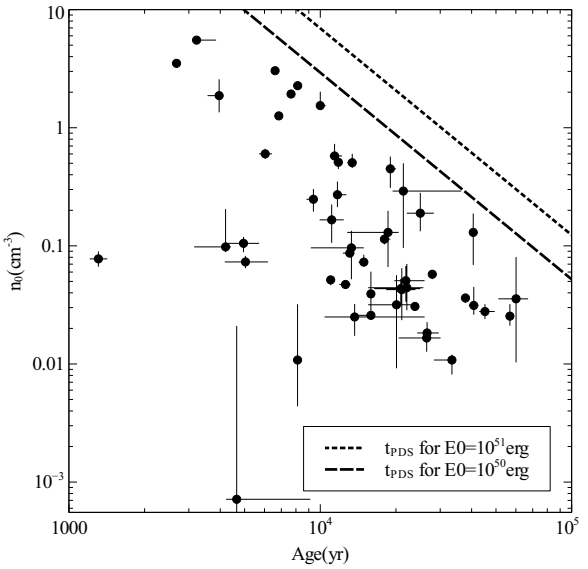

Fig. 1.— The derived densities vs. ages for the LMC SNRs (circles with error bars). The dashed and dotted lines show the theoretical transition time to the pressure-driven snowplow (PDS) phase, caused by radiative losses, for explosion energies of 10^{50} and 10^{51} erg.

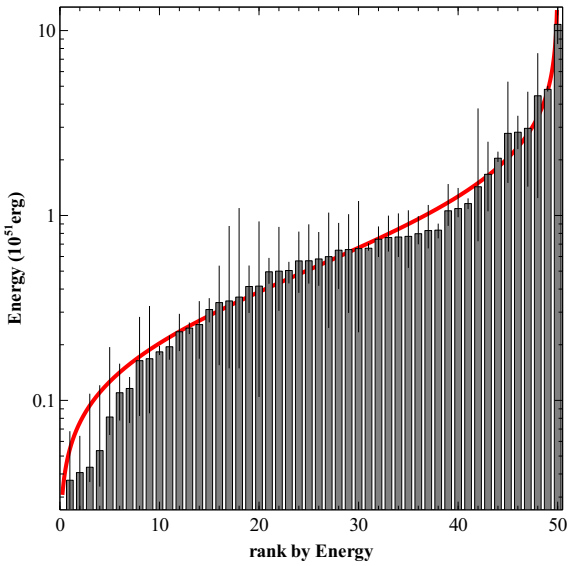

Fig. 2.— The cumulative distribution of explosion energies (histogram with error bars) for the LMC supernova remnant sample. The horizontal axis is the cumulative number of SNRs with energy less than or equal to the energy of a given SNR, the vertical axis is the energy of that SNR. The solid curve is a fit for the probability distribution expressed as a log-normal distribution (parameters given in the text).

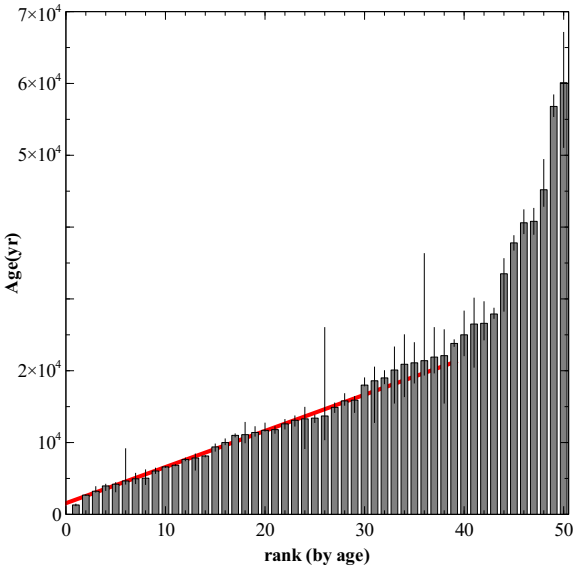

Fig. 3.— The cumulative distribution of ages (histogram with error bars) for the LMC supernova remnant sample. The solid curve is a linear fit equivalent to a constant birthrate of 1 per 503 yr. The fit is done for the 40 youngest SNRs in the sample.

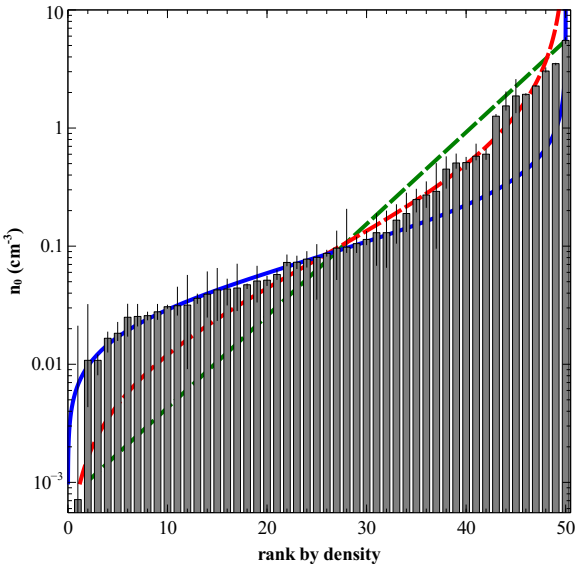

Fig. 4.— The cumulative distribution of circumstellar densities (histogram with error bars) for the LMC supernova remnant sample. The red and blue curves are fits to the probability distribution by a log-normal distribution. The solid blue curve is the fit to the low density part of the sample (lowest 30 densities) and the dashed red curve is a fit to the high density (highest 30 densities) part of the sample. A significantly worse fit to the density is by a n_0^{-1} probability distribution, shown by the green line.

TABLE 1
MODELS FOR LMC SNRS[a]

MCSNR	R(pc)	$E_0(10^{51}\mathrm{erg})$	E_0 error	age(yr)	age error	$n_0(\mathrm{cm}^{-3})$	n_0 error
J0449-6920	19.6	0.599	0.149/-0.351	21400	14900/-2000	0.291	0.209/-0.195
J0450-7050	41.2	2.96	1.33/-1.25	40600	1800/-1500	0.13	0.058/-0.0611
J0453-6655	31.0	2.78	0.42/-0.28	25000	3300/-2900	0.189	0.092/-0.056
J0453-6829	14.2	0.829	0.221/-0.112	11400	800/-500	0.577	0.153/-0.039
J0454-6626	12.8	0.164	0.057/-0.058	11100	1300/-1160	0.166	0.058/-0.06
J0505-6753	9.45	0.674	0.004/-0.009	6840	80/-60	1.28	0.02/-0.02
J0505-6802	11.6	1.06	0.2/-0.02	10000	500/-290	1.54	0.48/-0.12
J0506-6541	49.7	0.765	0.147/-0.095	56800	1600/-1400	0.0254	0.0067/-0.0043
J0506-7026	31.8	1.1	0.17/-0.01	15900	500/-1700	0.0258	0.0018/-0.002
J0508-6902	36.8	0.582	0.024/-0.01	26600	3000/-2300	0.0183	0.0043/-0.0024
J0508-6830	16.7	0.0871	0.0509/-0.0058	4650	4480/-430	.000715	0.0203/-0.000161
J0509-6844	3.60	0.116	0.003/-0.0312	3220	630/-120	5.52	0.29/-0.32
J0509-6731	3.75	0.037	0.0135/-0.01	3960	150/-400	1.87	0.7/-0.52
J0511-6759	13.6	0.0535	0.0448/-0.0191	8120	280/-270	0.0108	0.0212/-0.00642
J0512-6707	14.5	0.0407	0.0178/-0.0126	15900	100/-100	0.0392	0.0213/-0.0141
J0513-6912	29.1	0.654	0.114/-0.16	21100	2800/-2800	0.0426	0.0221/-0.0191
J0514-6840	26.7	0.246	0.002/-0.003	23800	500/-400	0.0307	0.0009/-0.0009
J0517-6759	39.3	0.662	0.018/-0.251	60100	7000/-9000	0.0356	0.0448/-0.0253
J0518-6939	17.9	0.37	0.039/-0.025	13300	1600/-4130	0.0962	0.0378/-0.044
J0519-6902	4.00	0.183	0.013/-0.001	2680	20/-40	3.51	0.02/-0.08
J0519-6926	23.0	0.744	0.032/-0.072	18000	1000/-100	0.114	0.019/-0.011
J0523-6753	21.8	0.504	0.017/-0.04	12600	600/-700	0.0471	0.0007/-0.0033
J0525-6938	13.4	4.81	0.13/-0.04	8130	70/-120	2.27	0.01/-0.01
J0525-6559	18.9	2.82	0.09/-0.08	11800	400/-500	0.51	0.054/-0.062
J0526-6605	10.2	1.16	0.04/-0.04	7650	190/-180	1.93	0.02/-0.03
J0527-6912	24.0	0.195	0.005/-0.008	27900	800/-600	0.0575	0.0049/-0.0052
J0527-6714	32.7	0.31	0.008/-0.01	37800	1000/-1000	0.0362	0.003/-0.0034
J0527-7104	44.7	0.568	0.037/-0.035	33400	100/-5100	0.0108	0.0012/-0.00265
J0528-6727	39.3	0.569	0.172/-0.049	40800	1800/-1800	0.0313	0.0136/-0.0052
J0529-6653	17.6	1.67	0.51/-0.44	5040	1150/-870	0.0731	0.0091/-0.0084
J0530-7008	39.4	0.4	0.013/-0.002	45200	4200/-2300	0.0278	0.0043/-0.0038
J0531-7100	19.6	0.496	0.035/-0.019	13100	600/-800	0.0868	0.0054/-0.0044
J0532-6732	34.5	1.68	0.23/-0.25	22100	3600/-6600	0.0442	0.0261/-0.0157
J0533-7202	24.9	0.31	0.028/-0.031	21900	4100/-2200	0.0507	0.0168/-0.017
J0534-6955	15.3	0.76	0.086/-0.007	13400	400/-600	0.506	0.096/-0.049
J0534-7033	22.5	0.833	0.031/-0.045	11000	200/-200	0.0515	0.004/-0.005
J0535-6602	9.80	2.04	0.08/-0.01	6610	60/-60	3.04	0.19/-0.06
J0535-6918	10.2	0.11	0.012/-0.009	9390	400/-580	0.248	0.055/-0.053
J0536-6735	23.6	0.797	0.05/-0.007	14900	600/-700	0.0728	0.0113/-0.0045
J0536-7039	21.8	0.168	0.038/-0.027	20900	4100/-4500	0.0434	0.0091/-0.0116
J0536-6913	6.54	0.0435	0.0301/-0.0035	4200	210/-1050	0.098	0.107/-0.0095
J0537-6628	27.5	0.415	0.12/-0.191	20100	3200/-4600	0.0317	0.0248/-0.0225
J0537-6910	14.5	10.8	0.1/-0.4	1310	110/-100	0.0776	0.0122/-0.011
J0540-6944	17.5	0.649	0.093/-0.156	19000	1000/-800	0.449	0.121/-0.139
J0540-6920	8.36	0.235	0.005/-0.008	6040	390/-330	0.601	0.062/-0.057
J0541-6659	36.4	0.5	0.146/-0.068	26500	3600/-6000	0.0166	0.0021/-0.0039
J0543-6858	40.0	4.44	0.95/-2.43	13700	12300/-3300	0.025	0.0072/-0.0077
J0547-6943	19.6	0.362	0.086/-0.042	18600	1900/-5800	0.13	0.068/-0.0638
J0547-6941	13.8	0.771	0.109/-0.122	4950	760/-660	0.105	0.014/-0.0166
J0547-7025	13.1	0.257	0.021/-0.049	11700	1000/-100	0.271	0.079/-0.058

[a]All models have SN ejecta mass of $1.4M_{\odot}$. R is the outer shock radius, E_0 is the explosion energy, n_0 is the pre-shock density.